Visual and Force-Feedback Guidance for Robot-Assisted Interventions in the Beating Heart with Real-Time MRI

Nikhil V. Navkar, Zhigang Deng*, Dipan J. Shah, Kostas E. Bekris, Nikolaos V. Tsekos*

Abstract— **Robot-assisted surgical procedures are perpetually evolving due to potential improvement in patient treatment and healthcare cost reduction. Integration of an imaging modality intraoperatively further strengthens these procedures by incorporating the information pertaining to the area of intervention. Such information needs to be effectively rendered to the operator as a human-in-the-loop requirement. In this work, we propose a guidance approach that uses real-time MRI to assist the operator in performing robot-assisted procedure in a beating heart. Specifically, this approach provides both real-time visualization and force-feedback based guidance for maneuvering an interventional tool safely inside the dynamic environment of a heart's left ventricle. Experimental evaluation of the functionality of this approach was tested on a simulated scenario of transapical aortic valve replacement and it demonstrated improvement in control and manipulation by providing effective and accurate assistance to the operator in real-time.**

I. Introduction

Improvements in the field of robot-assisted surgeries and image-guided interventions have led to the development of methodologies that promise to improve patient management and eventually contribute to the cost reduction of health care. The advent of real-time image guidance, especially combined with the accuracy and dexterity of robotic manipulators, offers new opportunities in the field of interventional medicine and can provide contextually rich information about the Area of Operation (AoO). Among the procedures, which can benefit from real-time guidance, are the intracardiac interventions, such as valvuloplasties, on the beating heart. Those, as well as other single access port surgeries are challenging since the interventional tool needs to be maneuvered by the operator inside the dynamic environment of the beating heart.

This work was supported by the National Science Foundation (NSF) award CPS-0932272. All opinions, findings, conclusions or recommendations expressed in this work are those of the authors and do not necessarily reflect the views of our sponsors. * denotes the co-corresponding authors of this work.

We would like to thank Karen Chin at the Methodist Hospital, Houston, TX for helping us to collect MR image data sets.

Nikhil V. Navkar is with the Computer Graphics & Interactive Media Lab and the Medical Robotics Lab at University of Houston, 4800 Calhoun Road, Houston, TX 77004, USA. nvnavkar@cs.uh.edu

Zhigang Deng is with the Computer Graphics & Interactive Media Lab and Computer Science Department, at University of Houston, 4800 Calhoun Road, Houston, TX 77004, USA. zdeng@cs.uh.edu

Dipan J. Shah is with Methodist DeBakey Heart & Vascular Center, Methodist Hospital, 6550 Fannin, Houston, TX 77030, USA. djshah@tmhs.org

Kostas E. Bekris is with the Computer Science & Engineering Department, University of Nevada, 1664 N. Virginia Street, Reno, NV 89557, USA. bekris@cse.unr.edu

Nikolaos V. Tsekos is with the Medical Robotics Lab and Computer Science Department at University of Houston, 4800 Calhoun Road, Houston, TX 77004, USA. ntsekos@cs.uh.edu

Real-time Magnetic Resonance Imaging (MRI) has emerged as one of the modalities for image-guided cardiac interventions ([1], and [2]). As compared to other imaging modalities, it offers the operator certain advantages, including: 1) volumetric imaging capabilities with a wide range of contrast mechanisms, 2) an inherent coordinate system of the MR scanner (acting as a reference frame for images and robot registration), 3) on-the-fly adjustment of imaging planes and the ability to track interventional tools, and 4) lack of ionizing radiations. However, real-time MRI-guidance requires the operator to perform the intervention in a confined space of MR scanner with a strong magnetic field and rapidly changing magnetic field gradients. In such a scenario, a robotic *telemanipulated* interventional system is useful as it facilitates real time imaging (i.e. the patient resides inside the MR scanner and images are collected in real-time), the patient is accessible remotely with the robotic manipulator, and the operator is at the vicinity of the scanner or even in the console room. This has led to the research and development of MRI compatible robotic systems ([3], [4]).

Several works have described and studied approaches for image-based guidance and control of robotic manipulators ([5], [6]). In case of cardiac surgeries, that involves a highly dynamic AoO, the majority of the work is based on the use of pre-operative image data ([7], [4], [8]). Park et al. [7] first introduced the innovative concept of virtual fixtures for cardiac surgeries (coronary artery bypass graft procedures) with the help of computed tomography (CT) images. Cine-MR images have also been used; for example Yeniaras et al. [4], described an approach that generated a dynamic deformable corridor inside the left ventricle that was safe for accessing the aortic root. Although cardiac cine-MRI generates high contrast images of a beating heart, it requires at least one breath-hold period, ECG triggering and several heartbeats to collect one set of multislice data for a cardiac cycle. Thus, cine-MRI is not suitable for real-time intraoperative analysis and thus often limited to preoperative surgical planning. An important contribution by Ren et al. [8] is to introduce the concept of dynamic virtual fixtures for minimally invasive robot assisted cardiac surgeries. The fixtures are generated by creating a visual-haptic model from preoperative dynamic MR/CT images and registering it using intraoperative ultrasound images. However, the spatial and temporal registration of preoperative image data with intraoperative images is a non-trivial task. Moreover, in the case of intracardiac interventions, the deformations secondary to breathing or beating-heart, as well as by the interventional tool (absent in the preoperative imaging data) also need to

be taken into consideration.

In this work, by utilizing fast MRI collected during the procedure to sense the AoO in real-time, we propose a novel guidance approach to assist the operator in performing robot-assisted transapical aortic valve replacement procedures. The guidance mechanism generates a dynamic guidance curve, which 1) acts as a path and provide visual cues to the operator in conjunction with real-time MR images, and 2) generates feedback forces on the controller of the telemanipulated robotic system to assist the motion of the manipulator in the right direction. The proposed method, in addition to providing visuo-force feedback guidance to the operator, can also generate appropriate control signals for a robotic manipulator.

II. Methods

A. Overview

This work describes an approach for human-in-the-loop control of robot-assisted interventions with real-time MRI guidance. Figure 1 shows its main components that integrate the patient, imaging modality, and the operator, via a computational core and visualization and force-feedback interfaces. The approach was evaluated for the clinical paradigm of TransApical - Aortic Valve Implant (TA-AVI), that involves the maneuvering of a prosthetic valve with an actuated manipulator, from the apex to the aortic annulus, via the Left Ventricle (LV). Our approach entails three steps:

- *Step 1*: Multislice oblique fast MR images (50 ms per image) are continuously collected to assess the motion of anatomical areas of interest pertinent to the procedure.
- *Step 2*: Those images are processed on-the-fly to generate a dynamically updated model of the AoO and to calculate a safe access path (through the beating LV).
- *Step 3*: This safe access path is used to update a virtual reality scene of the AoO, and drives a force feedback interface that is used by the operator for controlling a robotic manipulator.

In TA-AVI, the robotic manipulator is inserted though the apex ([1], [9]). To access the apex an incision is made on the chest and the pericardium is opened. Once the apex is exposed, a trocar is inserted into the LV. The trocar is either fixed to restrict the motion of the heart or is allowed to follow the motion of the apex. The robot is in form of a cylindrical tubular structure with prosthetic valve attached at the front. As the procedure is performed, the robotic manipulator is maneuvered by the operator inside the dynamically changing environment of LV towards the aortic annulus. The operator continuously perceives the changing environment of the AoO by analyzing the real-time MR images. In presence of only visual guidance (in form of two-dimensional MR images), the operator needs to ensure that the interventional tool does not collide and thus harm the moving endocardial wall and other vital anatomical structures (e.g., papillary muscles, mitral valve leaflets, and chordae tendinae) inside the LV. A guidance mechanism, in form of visual and force-feedback cues, would assist the operator to safely perform the procedure with anticipated outcomes.

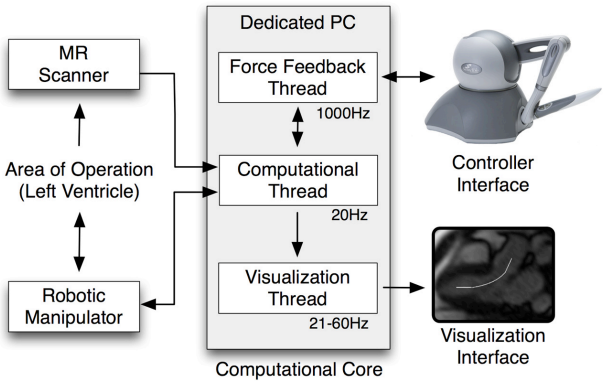

Fig. 1. Schematic illustration of the threads of the computational core running on a dedicated PC and their interaction with the MR scanner, the robotic manipulator, and the interfaces for the operator.

The system was tested on-line to assess the speed of data processing pipeline and off-line to assess its functionality. The following sections (II-B, II-C, II-D, and II-E) describe those steps and components in details.

B. MR Imaging and Image Processing

The dynamic AoO inside the beating heart is accessed with real-time MRI. To image different areas inside the beating heart (LV and aortic root) we implemented a MR acquisition protocol that collects non-triggered sets of three oblique-to-each-other MR slices. The slices are continuously collected in an interleaved fashion, i.e. *slice 1 - slice 2 - slice 3 - slice 1 - slice 2 - slice 3* etc, by using the processing pipeline proposed by Navkar et al. [10]. These three slices ($I_1(t)$, $I_2(t)$, and $I_3(t)$ described in Table I) are prescribed pre-operatively to depict the anatomical structures of interest in the AoO, that is, the endocardium in the LV and the aortic root.

TABLE I
Area Of Operation

Slice	Anatomical region depicted on the slice
$I_1(t)$	Long-axis view of apical region of the heart, mitral valve, aortic root, left ventricle, and left atrium.
$I_2(t)$	Long-axis view of apical region of the heart, mitral valve, left ventricle, and left atrium.
$I_3(t)$	Short-axis view of aortic annulus and left ventricle.

To accelerate the processing of MR data, the motion of the endocardium and aortic root on the respective slices are extracted using projection bands. Fig. 2 illustrates this approach, showing the respective projection bands and the monitored points of interest on the three slices ($I_1(t)$, $I_2(t)$, and $I_3(t)$). Once assigned pre-operatively on scout images, the projection bands are used to generate signal intensity projections [10]. The signals are further segmented to extract boundary points that correspond to the endocardium. In this work, each boundary point with index j that is extracted from slice i at time t is represented by $\mathbf{X_{i,j}}(t)$, where

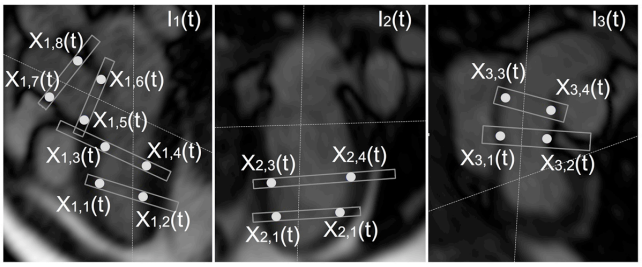

Fig. 2. The three imaging slices $I_1(t)$, $I_2(t)$, and $I_3(t)$ are collected in an interleaved fashion and without cardiac triggering. Their orientations are prescribed pre-operatively to image different anatomies. The dashed lines on a slice show the intersection with other slices. The rectangular boxes correspond to the operator specified projection bands. The dots within a projection band represent the boundary points that correspond to the endocardium.

$\mathbf{X_{i,j}}(t) \in R^3$. It is noted that all the computations are performed on-the-fly, i.e., as data is collected and passed to the dedicated PC that runs the computational core. In addition, all coordinates are calculated with respect to the inherent coordinate system of the MR scanner.

C. Generation of Safe Access Path

In this work, a safe access path in the form of a guidance curve is generated to assist the operator in both visualization and force-feedback based control of the intervention. A safe access path at a time instant t is represented by a curve $c(t)$.

To generate the curve $c(t)$, we first define four control curves $c_1(t)$, $c_2(t)$, $c_3(t)$, and $c_4(t)$ as shown in Fig. 3. The control curves are used to capture the motion of the tissue at the AoO. For transapical access to the aortic root, the control curves start from the apex of the LV (near the apical entrance) and extend up to the aortic root. They are computed by interpolating between the boundary points extracted from the real-time MRI. Here we explain the generation of one curve $c_1(t)$. The rest of the control curves are generated in a similar manner. The region between the boundary points $\mathbf{X_{1,1}}(t)$ and $\mathbf{X_{1,3}}(t)$, and $\mathbf{X_{1,5}}(t)$ and $\mathbf{X_{1,7}}(t)$ is linearly interpolated. Whereas, the region between the point $\mathbf{X_{1,3}}(t)$ and $\mathbf{X_{1,5}}(t)$ is interpolated using Kochanek-Bartels curves [11]. The tangential properties of these curves can be altered to adjust the deflection of the safe access path from the apical entrance to the aortic root. The operator sets the properties of the curve preoperatively. Depending upon the design of the robot and the anatomy of AoO, the curves can be deflected more towards the interventricular septum compared to the mitral valve and papillary muscles or vice versa.

The control curves are generated such that the number of interpolated points remains the same on each curve. The points on the guidance curve $c(t)$ are computed by calculating the average of the four points ($\sum_{i=1}^{4} c_i(t)/4$), each from a control curve, starting from apical region to the aortic root. Fig. 9 shows the guidance curve for different phases of a cardiac cycle.

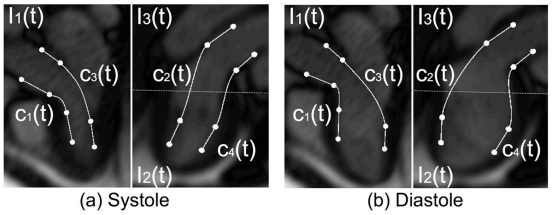

Fig. 3. Characteristic output example of the control curves on the slices $I_1(t)$, $I_2(t)$, and $I_3(t)$. The boundary points are interconnected to form the control curves. The motion of the endocardium is apparent for (a) systole and (b) diastole. It is noted that the curves $c_1(t)$ and $c_3(t)$ are on the imaging plane of slice $I_1(t)$, while the curves $c_2(t)$ and $c_4(t)$ are on the planes $I_2(t)$ to $I_3(t)$. All the points on the curve are measured with respect to the coordinate system of MR scanner.

D. Generation of Guidance Fixture

As the apex $\mathbf{X_A}(t)$ acts as a pivotal point for the robotic manipulator, it is important for the end effector $\mathbf{X_E}(t)$ to stay on the guidance curve $c(t)$ (illustrated in Fig. 4). In this work, the guidance curve $c(t)$ is used to implement a guidance virtual fixture at the controller's end of the telemanipulation system. A projection $\mathbf{X_P}(t)$ of the end effector $\mathbf{X_E}(t)$ is computed on the curve $c(t)$ such that:

$$\|\mathbf{X_E}(t) - \mathbf{X_A}(t)\| = \|\mathbf{X_P}(t) - \mathbf{X_A}(t)\| \tag{1}$$

Equation (1) ensures that the fixture does not cause any automated translation of the robotic manipulator. The force $\mathbf{F_1}(t)$ acting on the end effector is computed as:

$$\mathbf{F_1}(t) = k_1(\mathbf{X_P}(t) - \mathbf{X_E}(t)) \tag{2}$$

We also implemented a force profile $\mathbf{F_2}(t)$ that allows the operator to manipulate the controller freely when the end effector is at a closer proximity to the guidance curve. The normalized value of the force $\mathbf{F_2}(t)$ acting on the end effector is computed using an inverse Gaussian function [12] as:

$$\mathbf{F_2}(t) = (1 - e^{-k_2\|\mathbf{X_D}(t)\|^{k_3}})\frac{\mathbf{X_D}(t)}{\|\mathbf{X_D}(t)\|} \tag{3}$$

$$\mathbf{X_D}(t) = \mathbf{X_P}(t) - \mathbf{X_E}(t) \tag{4}$$

The variables k_2 and k_3 are used to generate different well-shaped force feedback profiles (as shown in Fig. 5).

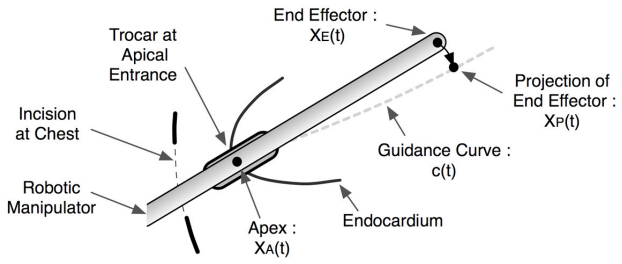

Fig. 4. Schematic illustration of a robot-assisted transapical cardiac intervention. A robotic manipulator is inserted through the trocar at the apical entrance near the incision on the chest.

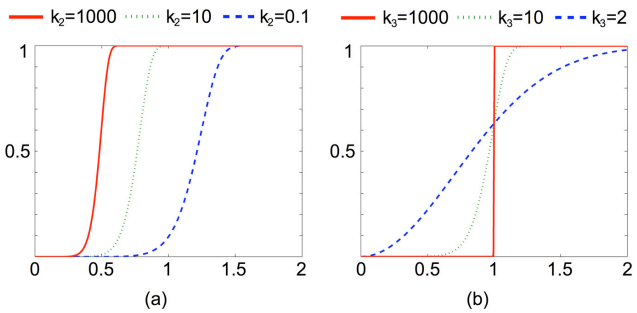

Fig. 5. The force profile $\|\mathbf{F_2}(t)\|$ for the distance $\|\mathbf{X_D}(t)\|$. In (a) the parameter k_2 is altered for $k_3 = 10$ and in (b) the parameter k_3 is varied for $k_2 = 1$.

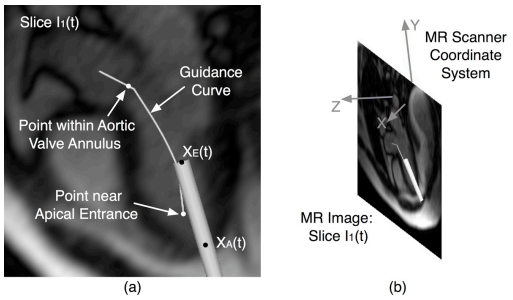

Fig. 6. Visualization of the AoO in the surgical task. The operator guides the end-effector of the robotic manipulator with the help of guidance curve. (a) The view displayed on the monitor. (b) The plane representing the MR image slice $I_1(t)$ is rendered with respect to MR scanner coordinate system. The viewing direction is along the $-Z$ axis of the coordinate system of MR scanner.

E. Multi-Threaded Processing

The code of the computational core was implemented using C/C++ with the Boost library for threading. All graphics rendering was done using openGL.

To achieve a high speed of processing, the three modules of the computational core of the system that compute the guidance curve, the visualization of AoO, and the generation of forces based on the guidance fixtures, respectively, are implemented as three dedicated threads that run in parallel on a PC (Intel 3.2 GHz processor with 9 GB RAM). The three threads (as shown in Fig. 1) are discussed below. The reported time durations or frequencies are with respect to this particular PC.

1) Computational Thread: This thread continuously receives data directly from the MR scanner (via TCP/IP) and (i) extracts boundary points from the projection bands (refer to step 1 in Section II-B) and (ii) computes the guidance curve from the boundary points (refer to step 2 in Section II-C). Those processes require less than 0.3 ms. Considering that each slice is refreshed every 50 ms, this thread does not add a significant overhead/delay; therefore, the frequency of this thread (including imaging) is $1/T_{ACQ}$ (i.e., 20 Hz), where T_{ACQ} is the acquisition time.

2) Visualization Thread: This thread receives real-time MR images and the dynamic guidance curve from the computational thread and generates the visualization scene of the AoO. The thread provides two modes of visualization. The first mode renders the guidance curve on top of the image slice $I_1(t)$ (an example is shown in Fig. 9). This mode provides a composite view of the AoO with vital anatomical structures pertinent to the intervention being rendered on a single slice display (the operator can select which slice). The second mode allows the inclusion of two or three images along with the guidance curve in a three-dimensional visualization space. The images are always rendered relative to the MR scanner coordinate system. The visualization thread runs asynchronously at speeds of 60 Hz and 21 Hz for the two modes, respectively.

3) Force Feedback Thread: The guidance fixture (step 2 described in Section II-D) is implemented with the force feedback thread. This thread runs at a high speed of 1 kHz suitable for a stable force feedback. In a single loop, this thread (i) receives the position of the end effector from the controller interface and the parameters of the guidance curve from the computational thread, (ii) computes the forces based on the projection of the end effector on the guidance curve and (iii) sends it back to the controller.

III. Experimental Studies

All the studies were performed on four healthy volunteers. Multislice, non-triggered and free-breathing MR images were collected with a true fast imaging with a steady-state precession (TrueFISP) via a Siemens 1.5T Avanto MR scanner. The acquisition time (T_{ACQ}) was 50 ms per slice, pixel size of 1.25×1.25 mm^2; FOV: 275×400 mm^2; matrix: 300x220; and slice thickness of 6mm. Considering heart rates of 60-80 bpm, in a single heart cycle we collected 20 to 25 MR images. The system was accessed with on-line studies to assess the speed of processing of the multithread implementation and identify possible bottlenecks.

The performance of the proposed guidance approach was evaluated with a visual/force-feedback interface connected to the aforementioned computational core. Our studies were performed off-line, i.e. with previously collected images that were managed by a virtual scanner that fed them into the computational core every 50 ms. The force feedback device was a three-degree of freedom Omni-Phantom (Sensable Technologies, Massachusetts, USA). The AoO is visualized on a high-definition LCD. The Omni-Phantom and the display were connected to the dedicated PC (as shown in Fig. 1). No robotic manipulator was connected to those studies that were focused only on the guidance aspect; any suitable robot could be controlled as the slave-side in a telemanipulated system.

The system was tested on the hypothetical scenario of TA-AVI. In reference to Fig. 6a, this involves guiding the end-effector $\mathbf{X_E}(t)$ of the robotic manipulator from a point near the apical entrance to a point within the aortic annulus. The end-effector was mapped onto the tip of the Omni-Phantom stylus. Furthermore, we assumed that the motion of the apex is constrained by the robotic manipulator (a valid assumption from the clinical point of view) and the apical entrance $\mathbf{X_A}(t)$ acts as a pivot point. The viewing direction

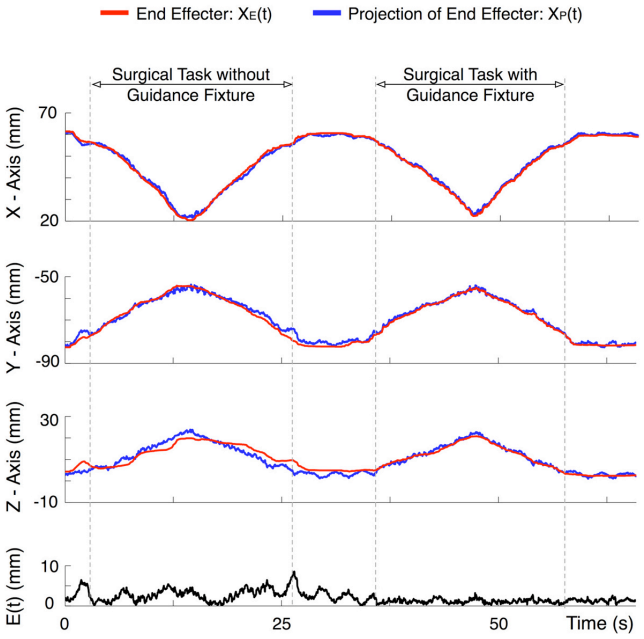

Fig. 7. Comparison of the position of the end effector $\mathbf{X_E}(t)$ and its projection $\mathbf{X_P}(t)$ measured for a surgical task with and without guidance fixture (and in presence of visual guidance). The displacements of the points are measured along the X, Y, and Z axes of the MR scanner coordinate system. The error $E(t)$ (in presence and absence of guidance fixture) for a surgical task is also shown.

(shown in Fig. 6b) is set parallel to the Z axis of MR scanner coordinate system.

We investigated and compared four guidance schemes:

- *No guidance*: The operator view the movie of the $I_1(t)$ MR slice rendered continuously on the monitor.
- *Visual guidance only*: The guidance curve $c(t)$ is rendered along with the corresponding real-time MR images of AoO. The curve acts as a trajectory and provides the operator with visual cues to maneuver the robotic manipulator.
- *Visual and force* $\mathbf{F_1}(t)$ *guidance*: In addition to the visual input, the operator is guided with the feedback forces exerted on the Omni Phantom using a force $\mathbf{F_1}(t)$ that varies linearly with distance from the guidance curve (Eq. 2). To generate adequate feedback forces for the controller, the value of k_1 is set to 0.2.
- *Visual and force* $\mathbf{F_2}(t)$ *guidance*: It is the same as the aforementioned *Visual and force* $\mathbf{F_1}(t)$ *guidance* scheme except it employs force-feedback profile $\mathbf{F_2}(t)$ computed from Eq. 3, where k_2 = 0.01 and k_3 = 10.

We used four measures of error: $E(t)$ that is the difference between the end effector position $\mathbf{X_E}(t)$ and its projection $\mathbf{X_P}(t)$ on the guidance curve, and $E_X(t)$, $E_Y(t)$, and $E_Z(t)$ that are the difference in the X, Y, Z coordinates of the points $\mathbf{X_E}(t)$ and $\mathbf{X_P}(t)$. Five volunteers were initially trained for nearly one hour on the visuo/force-feedback interface, to 1) understand the motion of the displayed virtual robotic manipulator and 2) map its motion with the controller interface (i.e. the Phantom-Omni). The displacement of the

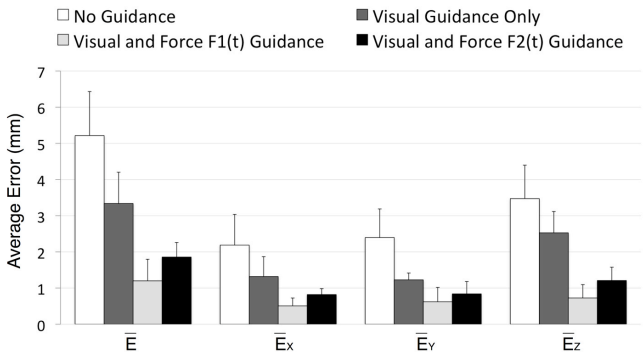

Fig. 8. Average errors ($\bar{E}$, $\bar{E}_X$, $\bar{E}_Y$, and $\bar{E}_Z$) measured over the duration of a surgical task for the four guidance schemes.

points $\mathbf{X_E}(t)$ and $\mathbf{X_P}(t)$ are also recorded along the axes of MR coordinate system.

IV. Experimental Results and Analysis

In all studies, our system generated paths (as shown in Fig. 9) that ensured a safe maneuvering inside the beating left ventricle; i.e. prevented collision to the walls of the endocardium. In a representative example, during end-systole (i.e. when the endocardial walls are at their closest position), the shortest distance of the path from from the endocardium to the apical region, base and aortic annulus were 10.7 mm, 12.5 mm, and 7.5 mm, respectively.

The performance of the individual modules and hardware components, as well as of the integrated system, was assessed during the course of the developmental phase. At the conclusion of this phase, volunteer operators assessed the functionality of the system. Figure 7 illustrates a representative result of such a study, showing the motion of the end effector and its projection performed by an operator for all the tasks. In the presence of force feedback and visual guidance, the error $E(t)$ decreases to 1.47 mm from 2.94 mm (when no force feedback guidance is used). The time required to perform the procedures in both the scenarios (i.e. with and without guidance fixtures) was nearly same ($\pm$7 second). The displacement of the points $\mathbf{X_E}(t)$ and $\mathbf{X_P}(t)$ were also recorded along the axes of the MR coordinate system. A subject whose skill-set is equivalent to that of an experienced operator for the given experiment, was able to guide the manipulator accurately along the X and Y axis direction in absence of guidance fixture. However, measurable errors occurred in Z axis direction. This representative result was primarily attributed to the difficulty of perceiving the spatial information, in particular depth, on a single two-dimension MR image. In such a case, the force feedback generated by the proposed guidance fixtures allows the operator to dynamically sense and rectify the position of the robotic manipulator. This clearly underscores the practical value of force feedback in human-in-the-loop robot control. It is noteworthy that based on the comments of the operators (experiment subjects), we feel that the Omni-Phantom device may not be an ideally intuitive interface as needed for such

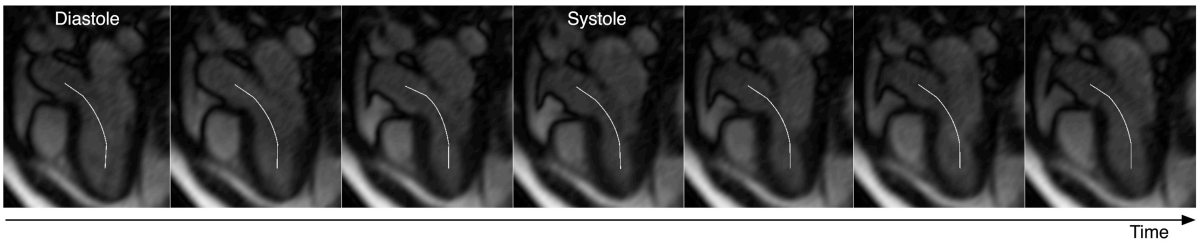

Fig. 9. Visualization of selected frames of a cardiac cycle showing the area of operation with dynamic guidance curve $c(t)$ on image $I_1(t)$.

tasks. Thus, it may be the case that novel force feedback devices need to be developed for such procedures.

The error values of combining visual and force feedback guidance for the four scenarios and for all the experiment subjects are illustrated in Fig. 8. This figure shows the mean of the average errors for the five subjects. The errors $\bar{E}$, $\bar{E}_X$, $\bar{E}_Y$, and $\bar{E}_Z$ are computed by taking the average of $E(t)$, $E_X(t)$, $E_Y(t)$, and $E_Z(t)$ for a given duration T of the surgical task ($\bar{E} = \sum_{t=0}^{T} E(t)/T$). With the addition of the proposed guidance mechanism, the average error decreases from 5.22±1.22 mm to 1.20±0.60 mm. With this visual force feedback guidance, a robotic interventional tool can be maneuvered inside the LV with a precision of less than 2 mm. This is equivalent to two-pixel spacing on a MR image representing the AoO. Although the results generated from the force profile $\mathbf{F_1}$ were more accurate as compared to $\mathbf{F_2}$, the later gave users more freedom to guide the tool.

V. Discussion and Conclusion

The work presents a guidance mechanism generated intraoperatively by an imaging modality for robot-assisted cardiac interventions. Real-time MR images are used to perceive the dynamic AoO that is sensed by rendering the information relevant to the operator via visual and force-feedback interfaces. Thus, integration of an imaging modality in a robotic surgical system would significantly improve its effectiveness and accuracy by providing real-time visual-force feedback assistance to the operator during the surgical procedure.

While the described approach can be potentially used with other modalities such as real-time ultrasound, MRI was chosen since it offers high contrast cardiac images, the ability to change the imaging planes on-the-fly electronically (without operator's interference) and the availability of different contrast mechanisms for assessing different aspects of tissue pathophysiology. However, as demonstrated in this work, acquiring MR images on-the-fly is a bottleneck for the processing pipeline. In this work, we used a speed of 50 ms per image, and this time can be further improved by reducing the acquisition time [13]. Another aspect of this work is the effect of the interventional tools on the images. When an interventional tool is placed inside MR scanner, the images (and hence the signal intensity projections) may be distorted, resulting in inaccurate guidance curves. In such a case, device-image interpretation enhancement techniques on real-time MR images [2] could be applied. When a robot with a specific kinematic structure and design is integrated with a real-time image guided telemanipulated surgical system, apart from guidance, issues such as transparency and stability also need to be considered in the bi-lateral telemanipulation. Though it would affect the way feedback forces are computed, our proposed guidance mechanism is still applicable.

References

[1] K. Horvath, M. Li, D. Mazilu, M. Guttman, and E. McVeigh, "Real-time magnetic resonance imaging guidance for cardiovascular procedures," *Seminars in thoracic and cardiovascular surgery*, vol. 19, pp. 330–335, 2007.

[2] M. Guttman, C. Ozturk, A. Raval, V. Raman, A. Dick, R. DeSilva, P. Karmarkar, R. Lederman, and E. McVeigh, "Interventional cardiovascular procedures guided by real-time mr imaging: an interactive interface using multiple slices, adaptive projection modes and live 3d renderings," *Journal of Magnetic Resonance Imaging*, vol. 26, no. 6, pp. 1429–1435, 2007.

[3] M. Li, A. Kapoor, D. Mazilu, and K. Horvath, "Pneumatic actuated robotic assistant system for aortic valve replacement under mri guidance," *IEEE Transaction on Biomedical Engineering*, vol. 58, no. 2, pp. 443 – 451, 2011.

[4] E. Yeniaras, J. Lamaury, N. Navkar, D. Shah, K. Chin, Z. Deng, and N. Tsekos, "Magnetic resonance based control of a robotic manipulator for interventions in the beating heart," in *ICRA'11*, 2011, pp. 6270 – 6275.

[5] M. Li, M. Ishii, and R. Taylor, "Spatial motion constraints using virtual fixtures generated by anatomy," *IEEE Transaction on Robotics*, vol. 23, no. 1, pp. 4–19, 2007.

[6] A. Bettini, P. Marayong, S. Lang, A. Okamura, and G. Hager, "Vision-assisted control for manipulation using virtual fixtures," *IEEE Transactions on Robotics*, vol. 6, pp. 953–966, 2004.

[7] S. Park, R. Howe, and D. Torchiana, "Virtual fixtures for robotic cardiac surgery," in *MICCAI'01*, 2001, pp. 1419 – 1420.

[8] J. Ren, R. Patel, K. McIsaac, G. Guiraudon, and T. Peters, "Dynamic 3-d virtual fixtures for minimally invasive beating heart procedures," *IEEE Transaction on Medical Imaging*, vol. 27, no. 8, pp. 1061–1070, 2008.

[9] K. Horvath, D. Mazilu, O. Kocaturk, and M. Li, "Transapical aortic valve replacement under real-time magnetic resonance imaging guidance: experimental results with balloon-expandable and self-expanding stents," *European Journal of Cardio-thoracic Surgery*, 2010.

[10] N. Navkar, E. Yeniaras, D. Shah, N. Tsekos, and Z. Deng, "Generation of 4d access corridors from real-time multislice mri for guiding transapical aortic valvuloplasties," in *MICCAI'11*, 2011, pp. 249 – 257.

[11] D. Kochanek and R. Bartels, "Interpolating splines with local tension, continuity, and bias control," in *Proc. of SIGGRAPH'84*, 1984, pp. 33 – 41.

[12] J. Ren and K. A. McIsaac, "A hybrid-systems approach to potential field navigation for a multi-robot team," in *ICRA'03*, 2003, pp. 3875 – 3880.

[13] E. McVeigh, M. Guttman, R. Lederman, M. Li, O. Kocaturk, T. Hunt, S. Kozlov, and K. Horvath, "Real-time interactive mri-guided cardiac surgery: Aortic valve replacement using a direct apical approach," *Magnetic Resonance in Medicine*, vol. 56, pp. 958 – 964, 2006.